Bioresource Technology 321 (2021) 124398

Contents lists available at ScienceDirect

Bioresource Technology

journal homepage: www.elsevier.com/locate/biortech

Electricity from methane by *Methylococcus capsulatus* (Bath) and *Methylosinus trichosporium* OB3b

Kalimuthu Jawaharraj [a,b,e], Saurabh Sudha Dhiman [b,c,e], Sierra Bedwell [d], Bhuvan Vemuri [a,b], Jamil Islam [a,b], Rajesh Kumar Sani [b,c,e], Venkataramana Gadhamshetty [a,b,e,*]

[a] Department of Civil and Environmental Engineering, South Dakota Mines, 501 E. St. Joseph Street, Rapid City, SD, USA
[b] BuG ReMeDEE Consortia, South Dakota Mines, 501 E. St. Joseph Street, Rapid City, SD, USA
[c] Chemical and Biological Engineering, South Dakota Mines, 501 E. St. Joseph Street, Rapid City, SD 57701, USA
[d] Department of Microbiology and Immunology, Montana State University, Culbertson Hall, 100, Bozeman, MT 59717, USA
[e] 2D-materials for Biofilm Engineering, Science and Technology (2DBEST) Center, South Dakota Mines, 501 E. St. Joseph Street, Rapid City, SD 57701, USA

HIGHLIGHTS

- Electricity generation from methane was demonstrated by model methanotrophs.
- A method of coating rGO/Ni electrodes with methanotrophs was developed.
- OB3b biofilms on rGO/Ni electrodes gave13-fold higher power.
- Bath biofilms on rGO/Ni electrode promoted methane oxidation.
- Cytochrome-based redox reactions were revealed in methane oxidation pathways.

GRAPHICAL ABSTRACT

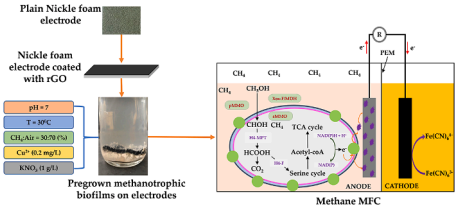

ARTICLE INFO

Keywords:
Electricity
Methanotrophs
Methane
Graphene
Extracellular electron transfer

ABSTRACT

Given the difficulties valorizing methane (CH_4) via catalytic routes, this study explores use of CH_4-oxidizing bacteria ("methanotrophs") for generating electricity directly from CH_4. A preconditioned methanotrophic biofilm on 3D nickel foam with reduced graphene oxide (rGO/Ni) was used as the anode in two-compartment microbial fuel cells (MFCs). This study demonstrates a proof of concept for turning CH_4 into electricity by two model methanotrophs including *Methylosinus trichosposium* OB3b and *Methylococcus capsulatus* (Bath). Both OB3b (205 $mW.m^{-2}$) and Bath (110 $mW.m^{-2}$) strains yielded a higher electricity from CH_4 when grown on rGO/Ni compared to graphite felt electrodes. Based on electrochemistry tests, molecular dynamics simulations, genome annotations and interaction analysis, a mechanistic understanding of reasons behind enhanced performance of methanotrophs grown on rGO/Ni are presented.

1. Introduction

Owing to the rapid expansion of oil and gas extraction across the world, there has been a rapid increase in the discharge of CH_4-rich natural gas into the environment (Shrestha et al., 2017). Along with the extraction activities, the oil and gas supply chains and transportation and storage facilities have resulted in ~8% CH_4 leaks into the environment (Howarth et al., 2011). Although chemical processes such as the Fischer-Tropsch process can valorize CH_4, they require a huge capital investment, expensive catalysts and external energy inputs (Haynes

* Corresponding author at: Department of Civil and Environmental Engineering, South Dakota Mines, 501 E. St. Joseph Street, Rapid City, SD, USA.
E-mail address: Venkata.Gadhamshetty@sdsmt.edu (V. Gadhamshetty).

https://doi.org/10.1016/j.biortech.2020.124398
Received 30 August 2020; Received in revised form 31 October 2020; Accepted 6 November 2020
Available online 12 November 2020

and Gonzalez, 2014). Indigenous microorganisms including aerobic methanotrophs can catalyze CH_4 oxidation under both aerobic and anaerobic conditions in the natural environments (Davamani et al., 2020).

Aerobic methanotrophs oxidize 30–99% of CH_4 in oxic environments (Bastviken et al., 2008; Yang et al., 2020). Owing to their fast growth kinetics, enhanced metabolic activity and robust performance in harsh environments (Roslev and King, 1995; Xin et al., 2020), methanotrophs are being sought for many environmental biotechnology applications (Jawaharraj et al., 2020a). This study explores the use of aerobic methanotrophs for generating electricity from CH_4 in MFCs. Prior MFC studies have used mixed cultures (McAnulty et al., 2017) based on methanotrophs or pure cultures of non-methanotrophs for oxidizing CH_4 (Slate et al., 2019).

Although mixed cultures are desirable for practical applications, there is a paucity of MFC studies on pure cultures of methanotrophs, specifically focusing on their extracellular electron transfer (EET) capabilities. Research efforts are also needed to identify gas-phase MFC bioreactor designs including electrode architectures for addressing classic challenges of low CH_4 solubility, mass transfer limitation, and slow biofilm growth. These design challenges are multiplied when methanotrophs are forced to use CH_4 as the sole carbon (C) source and respire onto the solid electrodes in MFCs.

This study presents a two-pronged approach for growing electrogenic biofilms of methanotrophs. First, the electrode surfaces were preconditioned in the presence of methanotrophic cells under optimal physiological conditions. Second, a biocompatible, conductive, porous nickel electrode modified with reduced graphene oxide (rGO/Ni) was developed to enhance the growth of electrogenic biofilms. The efficacy of this approach for enabling electricity generation from CH_4 by two model methanotrophs (OB3b and Bath) in MFCs (hereafter referred to as CH_4-MFCs) was evaluated in this study.

This is the first report on the previously unexplored exoelectrogenic capabilities of OB3b and Bath on rGO/Ni electrodes in MFCs fed with CH_4 as the sole carbon source. Although an earlier study by (Tanaka et al., 2018) demonstrated exoelectrogenic capabilities of *M. capsulatus*, their study used formate along with CH_4 as C substrates. Based on findings from electrochemistry tests, in-silico simulations, and heat map analysis, this study establishes extracellular electron transfer (EET) pathways of *M. trichosposium* and *M. capsulatus* species grown on rGO/Ni electrodes.

2. Materials and methods

2.1. Pre grown biofilms of model methanotrophs on electrode surfaces

2.1.1. Growth conditions

The OB3b cultures were grown in Nitrate Mineral Salts (NMS) medium using CH_4 as the sole C source. 80 mL of the NMS media (Bowman and Sayler, 1994) supplemented with 30 mL of 100 mM phosphate buffer and 10 μM of Fe (II) was transferred to 125 mL serum bottles. CH_4 along with air (1:1 v/v, 10 mL min^{-1}) was fed into the serum bottle for 7 days. These cultures were incubated at 30 °C at 200 rpm for 48 h. Under unoptimized conditions, inoculum cell mass was maintained at 1.5 mg mL^{-1}. The same procedure was used for growing Bath.

2.1.2. Optimization tests

The optimal conditions for the cell growth were determined using CH_3OH as the target product. The optimization parameters under consideration included temperature, pH, copper concentration, and agitation speed. These process conditions were used as input parameters in preconditioning tests.

2.1.3. Preconditioning and pregrown biofilms on electrodes

The biofilms were pregrown on a 2 cm × 2 cm graphite felt (GF) and rGO/Ni electrodes with a thickness of 0.4 cm and 0.16 cm, respectively. These electrodes were conditioned in a serum bottle containing the bacterial cultures and CH_4-supplemented NMS media for 7 days. The NMS media was void of any redox mediators. The preconditioned electrodes were used as anodes in CH_4-MFCs.

2.2. Methane-MFC

The test and control CH_4-MFCs were based on H-type MFCs described in an earlier study (Jawaharraj et al., 2020b). The volume of anode and cathode chambers was 200 mL each. The interelectrode distance was 0.005 m. CMI-7000 cation exchange membrane (Membranes International Inc, USA) was used a separator for anode and cathode. This membrane is a strong acid cation exchange membrane with its polymer structure made up of gel polystyrene and cross linked with divinylbenzene. These membranes were treated with 5% NaCl solution for 12 h to allow for hydration and expansion. A carbon brush (surface area of 130 cm^2) was used as a cathode and 50 mM potassium ferricyanide (in PBS buffer, pH 7.0) as the catholyte. An identical CH_4-MFC with nickel foam (NF) anode served as a control. The optimized conditions, as discussed in Section 1.1.2 were used in CH_4-MFCs. For example, both test MFCs and control were purged with CH_4: air (1:1 v/v) every 24 h. Methane levels in the headspace of CH_4-MFC were monitored periodically.

2.3. Bioelectrochemical measurements

The test CH_4-MFCs and controls were operated with an external load of 150 Ω using a fed-batch reactor protocol described in an earlier study (Jawaharraj et al., 2020b). Voltage data were obtained using a DAQ/54 module (I/O Tech Inc., Cleveland OH). External resistors (1 to 1,00,000 Ω; RS-200, IET Labs Inc., Westbury, NY) were used to calculate the operating voltage which was converted into current and power using Ohm's law. EIS analysis was performed using a Gamry reference 3000 potentiostat and with the following connections: the working electrode and working sense were connected to the anode; counter electrode and counter sense were connected to the cathode. EIS tests were performed at an open-circuit voltage (OCV), using an alternating current (AC) signal with an amplitude of 10 mV/sec, and frequency range of 0.01 Hz to 100000 Hz. The EIS spectra were obtained using the anode (rGO/Ni or graphite felt) as the working electrode (WE) and working sense electrode, the cathode (carbon brush) as the counter electrode (CE) and counter sense electrode. Ag/AgCl electrode was used as the reference electrode (RE). Gamry Echem Analyst software was used to analyze the EIS results using an external equivalent circuit fitting. The modified Randles circuit (E-Supplementary section) was used to determine the individual resistances in the system. Cyclic voltammetry was carried out using anode GF as the WE, Ag/AgCl was as the RE and cathode as the CE. Cyclic Voltammetry (CV) tests were carried out at a scan rate of 10 mV/s. The reproducibility of the impedance data was ensured by using a Kramers-Kronig (KK) compliant equivalent circuits.

2.4. Fabrication of reduced graphene oxide on nickel electrodes

NF (30 cm × 20 cm) and graphene oxide (GO) was purchased from MTI Corporation, USA and Sigma Aldrich, USA, respectively. The porous NF electrodes were characterized by a density of 346 g/m^3, an average hole diameter of 0.25 mm, 80–110 pores/inch, ≥95% porosity and 99.99% purity. Vitamin C that was used to reduce GO was purchased from Fisher Scientific, USA. Hydrochloric acid (HCl) used as a cleaning agent to remove the nickel oxide layer from the NF was also purchased from the Fisher Scientific, USA. Then rGO was impregnated onto the NF using the procedures discussed in previous studies (Chen et al., 2012; Islam et al., 2020). Briefly, NF was cut into 2.5 cm × 2.0 cm pieces, immersed in 6 M HCl and the mixture was sonicated for 10 mins to remove the unwanted nickel oxide layer and other impurities from the outer surface of NF. Deionized water (DI) (18.2 MΩ.cm) was used to

rinse the treated NF thoroughly.

6 mg mL^{-1} GO suspension was prepared by sonicating GO powder in DI water for 1 h. The pretreated NF samples were immersed in the GO suspension and agitated in a vortex mixer for 10 min and sonicated for another 10 min. The NF/GO suspension was transferred into a plastic tube (ø = 3 cm) containing 3.0 mL of 10 mg mL^{-1} vitamin C solution. The reaction chamber remained under ambient conditions overnight followed by heating at 60 °C for 2 h. The reaction tube was cooled down to room temperature and rinsed with DI water repeatedly. The rGO/Ni electrodes were dried at room temperature before use in CH_4-MFCs.

2.5. Biofilm and electrode materials characterization

The biofilm morphology of electrogenic methanotrophs was analyzed by scanning electron microscopy (SEM). The biofilm samples were fixed using 3% glutaraldehyde in a sodium cacodylate buffer (0.1 M, pH 7.2) using the procedures reported in the previous studies (Dedysh et al., 2015; Jawaharraj et al., 2020b). Electron micrographs of the acetone dehydrated biofilms on electrodes were captured using a Zeiss Supra40 SEM. A detailed structural and morphological properties of the rGO/Ni electrode were characterized using SEM and Raman spectroscopy. A ffTA Foram X3 module (Foster + Freeman Ltd, Evesham, UK) was used in Raman spectroscopy under a 10× lens magnification, power of 10 mW and laser excitation wavelength of 638 nm. The Raman spectrum was acquired between the wavenumber that ranged from 200 to 3700 cm^{-1} (Islam et al., 2020).

2.6. Expression profiling and gene interaction

The open-access source of OB3b genome was analysed using the https://genome.ucsc.edu/cgi-bin/hgGateway. The detailed information on the protein characteristics of the OB3b was processed using https://www.expasy.org/ and https://www.brenda-enzymes.org/. The online open-source service at https://rast.nmpdr.org/ and https://bioinfo-abcc.ncifcrf.gov/Heatmap/ was used to carry out genome annotations and interaction analysis. The functional heatmap was used to facilitate a robust clustering of genes based on expression profiles, heatmap visualization, and annotation of like groups together. Each panel in the primary heatmap encapsulated a sub pattern of the individual gene expression values unique to that data point.

2.7. Molecular dynamics (MD) and in-silico analysis

A BLAST search of the protein databank demonstrated the strongest similarity of the soluble MMO enzyme of Bath. X-ray crystal structure of sMMO from strain OB3b from the Protein Data Bank (ID: 1MHY) (https://www.rcsb.org/pdb/home/home.do) was used for energy calculations. The resulting model was also used for the substrate docking analysis (Basotra et al., 2019). For an in-depth analysis of enzyme-substrate interactions, methanol was used as a substrate analog for docking purposes. Hydrogen atom was added to the model followed by energy minimization to relax the confirmation from close contacts. Substrate ligand was docked using the CDOCKER, an MD simulated-annealing-based algorithm module. The structure of the substrate docked protein was subjected to energy minimization by applying CHARMm forcefield. Based on an energy docked confirmations, the substrate orientation which gave the lowest interaction energy was selected for further analysis (Zhang et al., 2012). MD simulation analysis was performed as described in the earlier study (Basotra et al., 2019). During methane oxidation and transfer of electrons from one center to another, Cyt-c has been reported to be actively coupled with various biomolecules. Cyt-c interacts with carbon monoxide while MMO oxidizes methane to other oxidation products. Regarding the methanol oxidation products, Cyt-c transfers the electrons from multiple sources while maintaining its favorable ionization energy. Thus, MD simulations were performed to study the molecular interactions between cytochrome protein and carbon monoxide. The sequence information of cyt-c protein was obtained from https://www.ncbi.nlm.nih.gov/protein/?term=cytochrome+C+methylosinus+trichosporium. For determining the binding coordinates and completeness of the protein structure, crystal structure of cytochrome cL from *Methylobacterium extorquens* (PDB ID: 2C8S) was used as template. The energy minimization of the structures was achieved using the CHARMm force field (Brooks et al., 1983). Molecular docking of the ligand was performed using the CDOCKER (Gagnon et al., 2016). The steepest descent and conjugate gradient methods were used to perform the simulations. All heavy atoms were minimized and fixed to relax the hydrogens. A heating phase (2000 steps: 300 K to 700 K) was designed followed by a cooling phase of 5000 steps to 300 K (Watowich et al., 1988). The simulations were continued at 300 K for 160 ps using 1-fs steps for completion.

3. Results and discussion

3.1. Pre grown biofilms of methanotrophs for methane oxidation

The optimal values for the growth of OB3b under aerobic conditions were determined via the process optimization studies (Table.1). Methanol yield was used as a target output in the optimization tests. The strain OB3b delivered maximum methanol concentration of 64 μM at temperature (T) = 30 °C (Table.1a) and 72 μM under neutral pH conditions (Table.1b). Other optimized parameter included copper concentration of 0.02 μM, yielding a maximum methanol concentration of 162 μM (Table.1c). The selected process variables were expected to influence the activity of sMMO and methanol dehydrogenase enzymes and subsequently the cell attachment and biofilm growth in CH_4 -MFCs.

The optimal values of the process variables were used for preconditioning GF and rGO/Ni anodes with OB3b biofilms. The preconditioned electrodes greatly reduced the start-up time and increased the performance of CH_4-MFCs with both the OB3b and Bath strains.

3.2. Electricity generation by methanotrophs using methane as the sole carbon source

Fig. 1(d-f) provides a proof of concept for electricity generation by OB3B using CH_4 as the sole C source. This is the first report on electricity generation by OB3B yielding 16 mW/m^2. The strain OB3B yielded an OCV of 0.3 V and a peak current density of 248 $mA.m^{-2}$ in CH_4-MFC,

Table 1
Bioprocess optimization studies for CH_4 oxidation by OB3b. Effects of temperature, pH and Cu concentrations in the methanol accumulation was evaluated using CH_4 as a sole source of carbon. Experiments were carried out in serum bottles and entailed the use of biological replicates (n = 2).

a. Temperature (°C)		Methanol accumulation (μM)
	20	23.6 ± 3.4
	25	44.2 ± 5.6
	30	63.7 ± 7.7
	35	59.6 ± 6.7
	40	34.5 ± 4.5
	45	29.6 ± 3.4
b. pH		
	5	22.7 ± 4.3
	6	60.7 ± 8.5
	7	72.3 ± 8.2
	8	54.1 ± 6.4
	9	33.6 ± 5.3
c. Cu concentration (μM)		
	0	141 ± 16.6
	0.01	145 ± 21.4
	0.02	162 ± 22.6
	0.05	155 ± 17.4
	0.1	140 ± 16.7
	0.2	145 ± 19.3

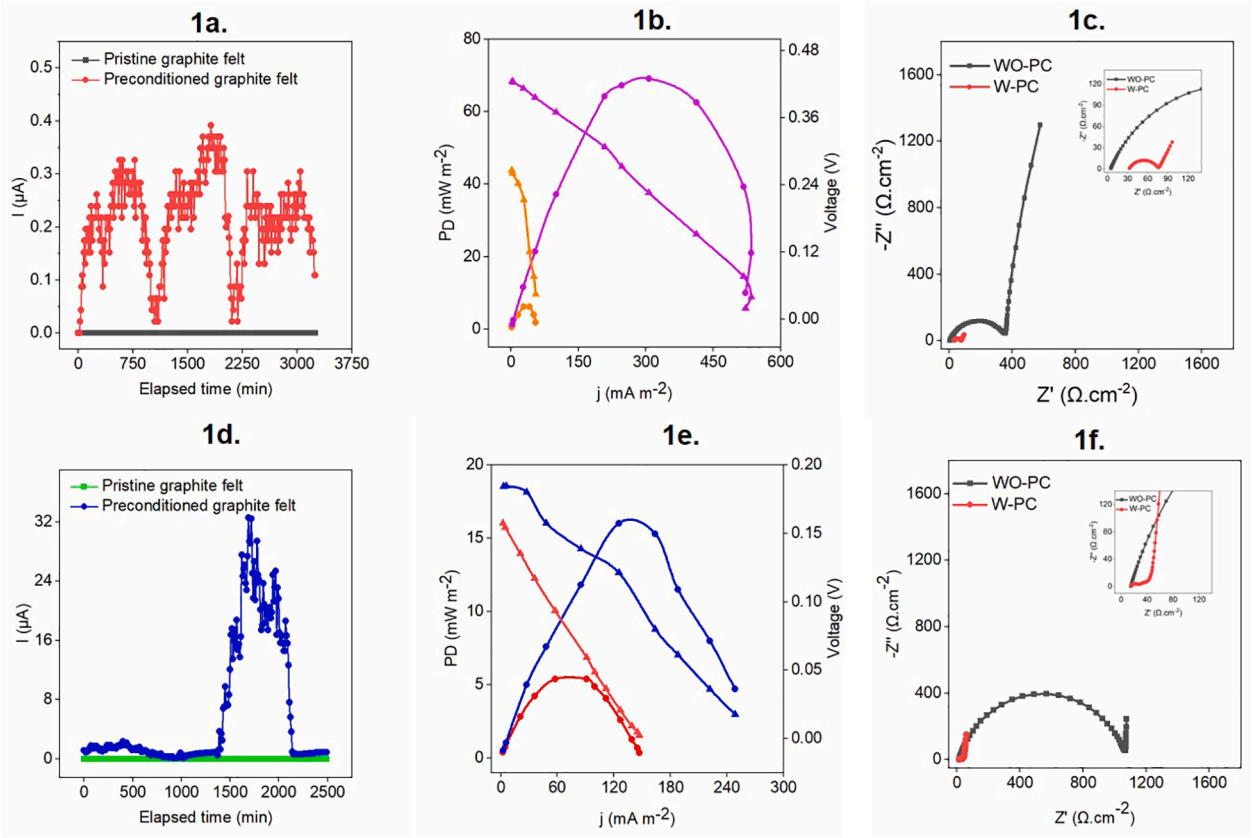

Fig. 1. Electricity production from CH_4 with pregrown biofilm of Bath (Top panel - Fig. 1a to c) and *Methylosinus trichosporium* OB3b (Bottom panel - Fig. 1d to f) in graphite felt electrodes. Current vs Time (Fig. 1a and d), polarization curves (Fig. 1b and e), Nyquist plots (Fig. 1c and f). Power densities denoted were Bath (W-PC); Bath (WO-PC); OB3b (W-PC); OB3b (WO-PC). Voltages denoted were Bath (W-PC); Bath (WO-PC); OB3b (W-PC); OB3b (WO-PC). WO-PC – without preconditioning; W-PC – with preconditioning.

operated under the optimal growth conditions (Table 2). An abiotic control MFC (plain NF and GF) did not generate any noticeable electric current from CH_4 oxidation (not discussed further). The potential extracellular transfer mechanisms of the OB3b are further discussed in Section 2.6.

The pregrown OB3b biofilm on electrodes enhanced the performance of CH_4-MFCs. The power output (16 $mW.m^{-2}$) of CH_4-MFC with the preconditioned CF electrode was 3.2-fold higher than that of planktonic cells (Fig. 1d-f), for the entire experimental duration (shown in the I vs T plot, Fig. 1d). This study also demonstrates the ability of Bath to generate electricity (534 $mA.m^{-2}$) using CH_4 as the sole C source (Table 2, Fig. 1a-c).

The performance of the strain OB3b was lower than Bath under identical CH_4-MFC conditions. Although, both the OB3B and Bath strains yielded similar OCV values (0.3 V and 0.26, respectively), the peak power density for Bath on the GF anode (69 $mW.m^{-2}$) was 4.3-fold higher than OB3b (16 $mW.m^{-2}$). The peak current density of Bath (534 $mA.m^{-2}$) was also 2.2-fold higher than OB3b (248 $mA.m^{-2}$). However, as discussed in Section 2.4, this trend reversed when rGO/Ni was used as an anode, where the strain OB3B outperformed Bath.

M. capsulatus features a "Cu switch" mechanism which affects the genetic expression of pMMO, sMMO and outer membrane cytochrome proteins (Semrau et al., 2018; Tanaka et al., 2018). Also, Cu deficient *M. capsulatus* cells have been reported to produce a 5-fold higher current (118 $nA\ cm^{-1}$) compared with the Cu supplemented cells. This result has also been substantiated by the elevated levels of OMC gene expression, enhancing EET to the electrodes (Tanaka et al., 2018). This report by Tanaka et al., 2018 on OMC proteins of *M. capsulatus* remains the first report on methanotrophic (aerobic) OMCs at the pure culture levels. Future researches are warranted to illustrate the exact mechanism in *M. capsulatus*.

The EIS results based on the Nyquist plots corroborated the findings from the polarization tests (Fig. 1c and f). The charge transfer resistance (R_{CT}) at the electrode–electrolyte interface is directly proportional to the diameter of the semicircle in Nyquist plots. This study indicated that Day 7 in CH_4-MFC showed far lesser resistance compared to Day 1, indicating that the pregrown biofilm thrived in the CH_4-MFC environment. The Nyquist data was then fitted into an electrical circuit to quantify different types of resistances (Tables 3 and 4). The total internal resistance in CH_4-MFC using Bath was found to be 369.5 ± 5.09 $\Omega.cm^2$ (day 1) and 76.2 ± 1.56 $\Omega.cm^2$ (day 7). Whereas in the case of OB3b, the total resistance was 1076.85 ± 12.18 $\Omega.cm^2$ (day 1) and 45.6 ± 1.8 $\Omega.cm^2$ (day 7).

These results revealed that the preconditioned biofilms showed 4.8-folds and 23.6-folds lesser resistances (than electrodes without

Table 2
Comparison of methane-MFC using OB3b and Bath methanotrophs from this study using graphite felt and rGO/Ni electrodes.

Methanotrophs	Electrodes	Electron donor	OCV (V)	Peak power density ($mW.m^{-2}$)	Peak current density ($mA.m^{-2}$)
M. trichosporium OB3b	Graphite felt	CH_4	0.3	16	248
M. trichosporium OB3b	rGO/Ni foam	CH_4	0.36	205	1538
M capsulatus Bath	Graphite felt	CH_4	0.26	69	534
M. capsulatus Bath	rGO/Ni foam	CH_4	0.32	110	698

Table 3
EIS fitting results showing the different resistances in MFC using OB3b (GF and rGO/Ni electrodes). WO-PC – without preconditioning; W-PC – with preconditioning.

Resistances (Ω.cm^2)	OB3b (GF)		OB3b (rGO/Ni)	
	WO-PC	W-PC	WO-PC	W-PC
R_{soln}	14.85 ± 0.14	13.47 ± 384.3e-3	22.1 ± 0.6518	6.7 ± 0.1979
R_{ct}	1062 ± 12.04	32.13 ± 1.779	21.8 ± 1.905	8.1 ± 1.401
Total resistance	**1076.85 ± 12.18**	**45.6 ± 1.8**	**43.9 ± 2.6**	**14.8 ± 1.6**

Table 4
EIS fitting results showing the different resistances in MFC using Bath (GF and rGO/Ni electrodes). WO-PC – without preconditioning; W-PC – with preconditioning.

Resistances (Ω.cm^2)	Bath (GF)		Bath (rGO/Ni)	
	WO-PC	W-PC	WO-PC	W-PC
R_{soln}	4.5 ± 0.06883	31.94 ± 0.4881	15.17 ± 0.2083	6.26 ± 0.04439
R_{ct}	365 ± 4.950	44.26 ± 1.074	14.37 ± 2.26	30.37 ± 2.38
Total resistance	**369.5 ± 5.09**	**76.2 ± 1.56**	**29.54 ± 2.47**	**36.6 ± 2.39**

preconditioning) in CH_4-MFC driven by Bath and OB3b, respectively. Even though OB3b showed a 23.6-fold decrease in total resistance, it does not display a higher power density like Bath (Table 2). Interestingly, an excessive growth of OB3b biofilm was observed on the graphite felt anode, as evident from the SEM images (E-Supplementary section). This excessive growth can be attributed to non-conductive debris including dead cells on the anode surface, reducing the overall power output (Slate et al., 2019).

3.3. Characterization of reduced graphene oxide on nickel electrodes

The SEM images displayed a typical honeycomb structure for the pristine NF electrodes. For the rGO/Ni electrodes, the micropores of the honeycomb were filled uniformly with rGO. The presence of graphene and the crystal defects in graphene structures is typically designated by G and D peaks respectively. The peak position of the G band lies between 1575 and 1595 cm^{-1} and 1325–1340 cm^{-1} for the D band (Islam et al., 2020; Kumar et al., 2014). The previous results showed that G band increased significantly in rGO/Ni compared to GO. Typically, G, D and 2D bands are the Raman signatures of graphene. Hence, the blue shift of the 2D band from 2632 cm^{-1} (GO) to 2727 cm^{-1} (rGO/Ni) indicated the surface adhesion of rGO on NF. Moreover, high intensity of υ_s (C–H) in rGO/Ni suggests that the basal plane of graphene/rGO contains plenty of hydrogen atoms that were contributed by functional groups (–OH, –COOH and –CO). These functional groups turned the hydrophobic NF surface into a hydrophilic surface (Islam et al., 2020). The ratio of the intensity of 2D and G peaks (I_{2D}/I_G) for rGO/Ni (0.80) was 2.28-fold higher compared to GO (0.35), suggesting the existence of multi-layer graphene layers. The chemical exfoliation process of rGO from GO offers a low yield; therefore few layers of reduced graphene oxide were produced on the NF (Priyadarsini et al., 2018).

3.4. Enhanced performance of methane-MFC with reduced graphene oxide-nickel electrodes

A rationally designed rGO/Ni was found to promote the cell attachment and EET capabilities of methanotrophs. For OB3b, the peak power density of rGO/Ni anode (205 mW.m^{-2}) was 12.8-fold higher than GF (16 mW.m^{-2}). For Bath, the peak power density of rGO/Ni anode (110 mW.m^{-2}) was 1.6-fold higher than GF (69 mW.m^{-2}) (Fig. 2b and f). Whereas the peak current densities were reported to be 698 mA.m^{-2} and 1538 mA.m^{-2} for Bath and OB3b, respectively. This revealed that OB3b yielded a 1.9-fold increase in power densities than Bath. This implies that engineered rGO/Ni anodes favored the growth of OB3b biofilms compared to Bath. CH_4-MFCs using rGO/Ni anodes showed steady-state performance for the entire experimental duration (shown in the I vs T plot, Fig. 2a and e).

The rGO/Ni anodes yielded 12.8 and 1.6-folds higher power densities compared with GF anodes (Table 2). This is substantiated by the EIS analysis of the Nyquist data where the preconditioned biofilm (Day 7) showed far lesser resistance than electrodes without preconditioning (Day 1) (Fig. 2c and g). The total internal resistance of OB3b was found to be 43.9 ± 2.6 Ω.cm^2 (day 1) and 14.8 ± 1.6 Ω.cm^2 (day 7) and. In the case of Bath, the total resistance was 29.54 ± 2.47 Ω.cm^2 (day 1) 36.6 ± 2.39 Ω.cm^2 (day 7) and, respectively (Tables 3 and 4). These results revealed that preconditioned OB3b biofilms showed 3-folds lower resistances (than day 1) and there is no significant differences in resistance values of Bath biofilm. This corroborates the higher power densities in OB3b/rGO-Ni MFCs than the Bath system. The rGO/Ni electrodes were also reported to promote the biofilm formation, EET mechanisms and methylotrophic capabilities of *Rhodobacter sphaeroides* 2.4.1. strain based on a previous study (Islam et al., 2020). Reports on GO-based anodes for enhancing the methanotrophic capabilities are scarce. However, 3D rGO-based electrodes have been reported to enhance the performance of a batch MFCs driven by *Shewanella oneidensis* (Wang et al., 2013).

Cyclic voltammograms were recorded to determine the biocatalytic performances of the methanotrophs at a scan rate of 50 mV/s (Fig. 2d and h). The CVs of Bath and OB3b on rGO/Ni electrodes displayed oxidation and redox peaks at −0.28 mV and −0.21 mV (vs Ag/AgCl), respectively. Interestingly, the oxidation peak current in the OB3b (rGO/Ni) (0.0167 mA) was 3.3-fold higher compared to Bath (0.005 mA), suggesting enhanced CH_4 oxidation by OB3b. The oxidation peak for both the OB3b and Bath at −0.2 V (vs Ag/AgCl) can be attributed to the methane and methanol oxidation process (Anthony, 1986).

3.5. Heat map analysis

The expression pattern was assessed for the genes encoding the essential enzymes for the CH_4 oxidation (Fig. 3). A significant upregulation (FPKM log value) was observed in the MMO enzyme, as it is the primary oxidizer of the assimilated CH_4. The upregulation of the MDH could be correlated with the cellular assimilation of the accumulated methanol, which gets converted into formaldehyde by MDH (Al-Taho et al., 1990; Mcdonald and Murrell, 1997). In the case of OB3b, a complete serine cycle is present, regulating the synthesis of numerous metabolites required for the biomass growth (Hanson and Hanson, 1996). Therefore, the upregulation of the genes encoding for the malyl-CoA lyase, phosphoenolpyruvate carboxylase enzyme, etc. exhibits the subsequent assimilation of the CH_4 oxidation products. The malyl-CoA lyase enzyme controls the terminal stage of the serine cycle. It resulted in the formation of acetyl Co-A, which itself is a precursor for numerous cellular metabolites. Therefore, the upregulation of the malyl-CoA lyase is crucial for the growth of the OB3b in CH_4 rich conditions (Fig. 3).

Likewise, the upregulation in several essential genes governing the N-metabolism in OB3b was observed. The cytochrome-c oxidase is a large transmembrane protein involved in the transfer of electrons from ferrocytochrome (Harbitz and Andersson, 2011). An upregulated cyt-C is essential for the rapid movement of the electron, which determines the strength of current density. Likewise, the ubiquinone reductase is directly involved in the e-transfer, and its upregulation exhibits the attainment of the optimum conditions, which in turn favored the increased rate of electron transfer and increased electricity production.

The role of the MDH in N-metabolism and electron transfer is crucial

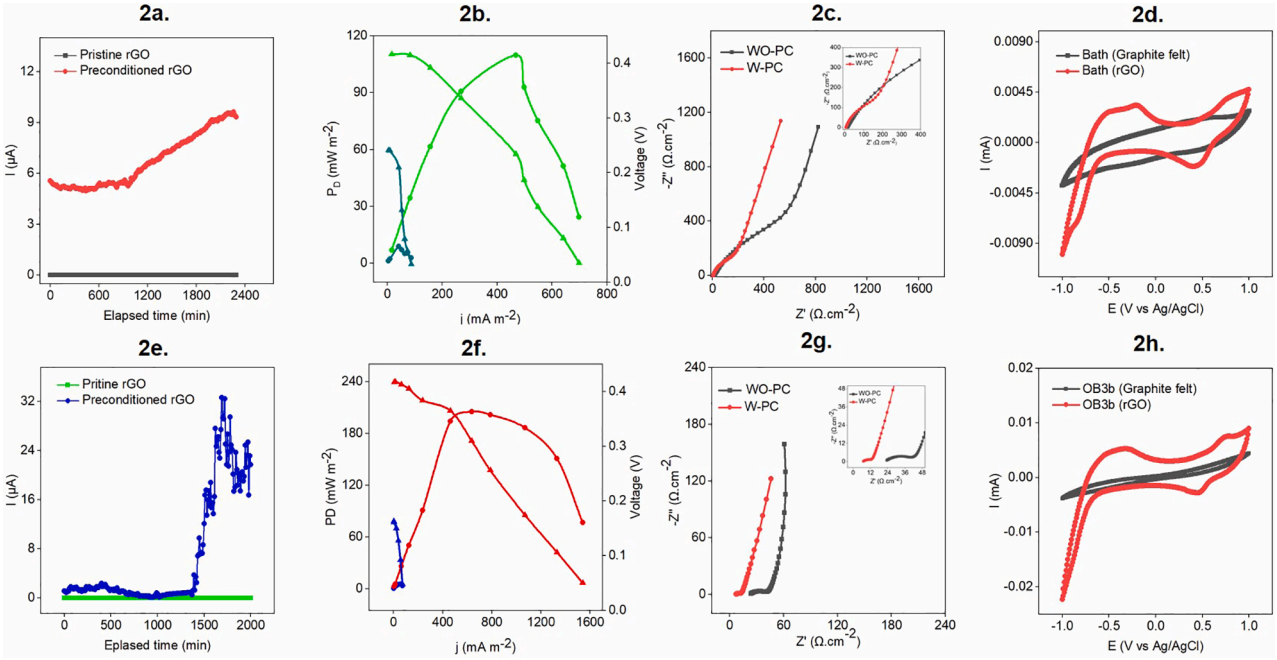

Fig. 2. Materials engineering strategy for enhanced electricity production from CH_4 by Bath (Top panel - Fig. 2a to d) and OB3b (Bottom panel - Fig. 2e to h) using rGO/Ni electrodes. Current vs Time (Fig. 2a and e), polarization curves (Fig. 2b and f), Nyquist plots (Fig. 2c and g), cyclic voltammograms (Fig. 2D and h). Power densities denoted were Bath (W-PC); Bath (WO-PC); OB3b (W-PC); OB3b (WO-PC). Voltages denoted were Bath (W-PC); Bath (WO-PC); OB3b (W-PC); OB3b (WO-PC). WO-PC – without preconditioning; W-PC – with preconditioning.

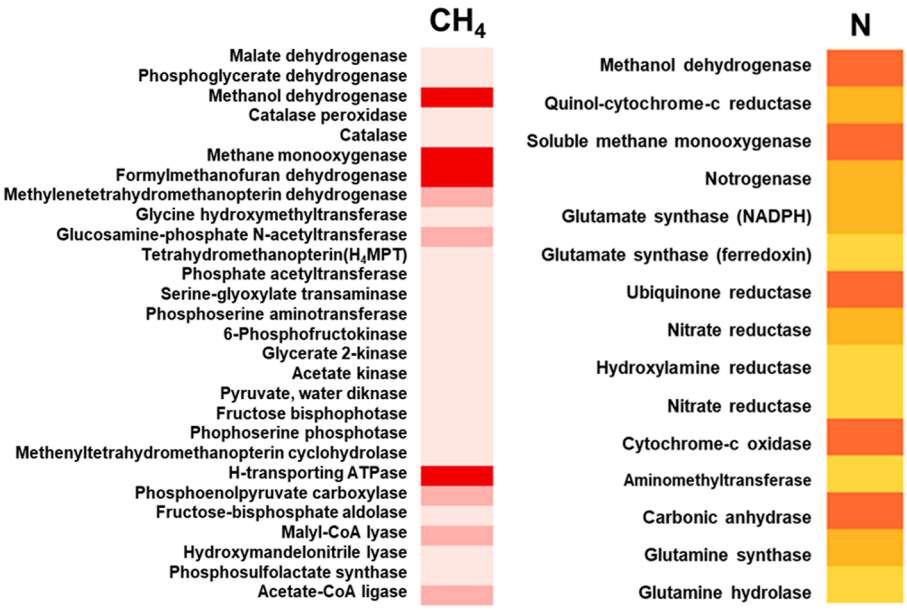

Fig. 3. Heatmap of protein families involved in methane, nitrogen and carbon metabolic pathways of OB3b.

for the growing biomass. MDH is in the group of enzymes that harbors the pyrroloquinoline quinone (PQQ) as their prosthetic group. The entire protein complex is made up of catalytic subunits, with PQQ as their redox center, and electron acceptors, such as cyt-C, which transfer electrons from reduced PQQ to the respiratory chain. Therefore, the upregulation of the gene encoding the MDH enzymes is critical for the complete oxidation of CH_4 and the transfer of electrons.

3.6. Potential pathways of methane oxidation into electricity by M. trichosporium

The OB3b features both pMMO and sMMO enzymes for oxidizing CH_4. The Cu^{2+} levels (>3 μm) used in this study are expected to allow OB3B to switch to the pMMO mediated CH_4 oxidation. The OB3b can fix the environmental nitrogen, as corroborated by the expression profile of different enzymes that gets upregulated during the standardized N-conditions (Fig. 3).

In this study, OB3b was grown under copper-free concentration to

confirm the rate of CH_4 oxidation by sMMO. The product of CH_4 oxidation (i.e., methanol) is converted to formaldehyde by PQQ-dependent methanol dehydrogenase (MDH). The MD simulations revealed the molecular interactions between methanol and MMO hydroxylase subunit, a crucial step for liberating methanol and sustaining CH_4 oxidation in OB3b cultures (E-Supplementary). Based on the lowest discrete optimized protein energy (DOPE) score values, a suitable docking pose for methanol substrate to interact with the MMO hydroxylate subunits were determined (shown in green color). The selection criteria are based on the lowest discrete optimized protein energy (DOPE) scores and other details of the MD simulations (E-Supplementary section).

An in-silico approach was used to analyze three different aspects viz. (i) ligand docking for binding orientations, (ii) distance between interacting atoms of ligand and enzyme, and (iii) statistical data of substrate binding orientation. The binding site coordinates of the PDB ID 2C8S were used for docking of the substrate analog. The charge distribution at the binding site of the protein is shown in E-Supplementary section. The carbon monoxide (CO) was used as the substrate analog to define the readiness of the cyt-c protein towards donation of the electron for subsequent oxidation of as produced methanol by the MMO enzymes (Ferenci, 1974; Tonge et al., 1974). Additionally, ionization energy and pKa values of the biomolecule significantly affects their function as an electron donor (Lucas et al., 2011). The basicity of the surrounding environment facilitates the electron donor characteristics of the biomolecule (Dwyer, 2005). Using in-silico analysis the ionization properties of the cyt-c was determined and the vicinity of the interaction residue (Glu124) facilitates the transfer of electron while interacting with the substrate analog (E-Supplementary section). Electrostatic interaction was determined between the sp^2 hybridized O-atom of the protein molecule with the substrate analog. Interaction which are occurring within the 5A range were analyzed due to their potential influence on the ligand orientation.

The activity of the enzyme *in vivo* requires cytochrome cL and several chaperones, regulators, and enzymes, including genes required for Ca^{2+} insertion. Previous enzymatic studies predict three possible pathways for formaldehyde oxidation: (1) direct oxidation through dye-linked heme-containing formaldehyde dehydrogenase, (2) H4folate-, and (3) H4MTP-mediated C1 transfers. This reaction step is mediated by the three broad-specificity aldehyde-detoxification systems, including two NAD-dependent aldehyde dehydrogenases and one aldehyde oxidase.

Multiheme c-type cytochrome complex proteins, the essential outer membrane proteins (Tokunou et al., 2016) along with the pili assembly proteins (Zhou et al., 2018) are involved in EET from the cell membrane to the electrodes in electrogens. The OB3b genome constitutes of about ten putative c-type cytochromes but only few of them were annotated (Harbitz and Andersson, 2011). Among them, a homolog of cytochrome *c*-554 among the cytochrome c2 of OB3b has been reported to mediate electron transfer between cytochrome *c* oxidases and bc1 complex (Bertini et al., 2006). The recent reports (Naizabekov and Lee, 2020) suggested a genome-scale metabolic reconstruction of OB3b with ubiquinol acting as an electron donor for methane oxidation; whereas methanol dehydrogenase gives electrons to complex IV directly through cytochrome *c*.

Based on the above, this study proposes an extracellular electron transfer pathway for OB3b as shown in Fig. 4. This type of electron transfer has been suggested recently for a type II methanotroph *Methylocystis* sp (Bordel et al., 2019a, 2019b). Further studies are warranted to explore the exact genetic mechanism of extracellular electron transfer of OB3b to anodes.

4. Conclusions

This study provided a proof of concept for electricity generation by two model methanotrophs under sub-oxygen levels in MFCs. Using the gene expression analysis and MD simulations, the key genes were identified to be involved in CH_4 oxidation and electricity generation from CH_4 by a less explored OB3b. To overcome technical barriers of using a low solubility CH_4 gas as the C source in CH_4- MFCs, a first step would be to promote the growth of methanotrophs on the electrode surfaces. This study addressed this challenge partially by combining electrode surface engineering approaches and biofilm growth techniques.

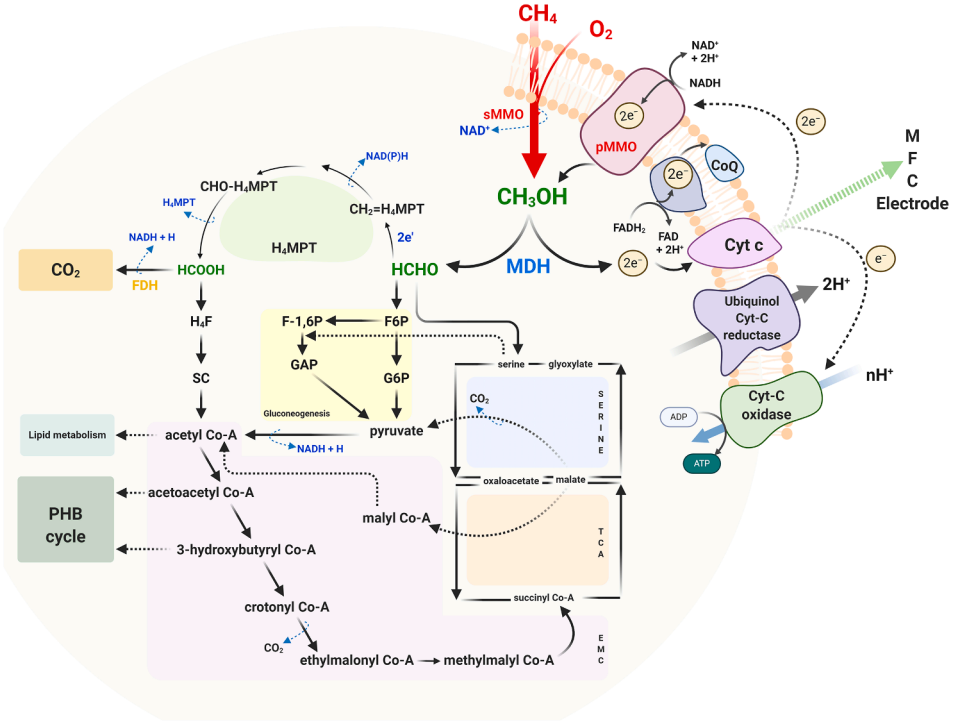

Fig. 4. Potential mechanism of methane oxidation and electricity generation by OB3b. Both pMMO and sMMO enzymes are involved in methane oxidation whereas, methane is converted to formaldehyde by PQQ-dependent methanol dehydrogenase. Followed by which formaldehyde can be oxidized using three different ways i.e., 1. Direct oxidation; 2. Tetrahydrofolate (H4F); 3. H4MTP-mediated C1 transfers. Besides, ubiquinol acting as an electron donor for methane oxidation whereas methanol dehydrogenase giving electrons to complex IV directly through cytochrome *c* (Naizabekov and Lee, 2020). This study proposes that cytochrome *c* oxidase along with ubiquinol cyt-c reductase might be involved in extracellular electron transfer to anodes on CH_4-MFCs.

CRediT authorship contribution statement

Kalimuthu Jawaharraj: Conceptualization, Validation. **Saurabh Sudha Dhiman:** Conceptualization, Validation. **Sierra Bedwell:** Conceptualization, Validation. **Bhuvan Vemuri:** Visualization. **Jamil Islam:** Visualization. **Rajesh Kumar Sani:** Conceptualization, Supervision, Validation, Project administration, Funding acquisition. **Venkataramana Gadhamshetty:** Conceptualization, Supervision, Validation, Project administration, Funding acquisition.

Declaration of Competing Interest

The authors declare that they have no known competing financial interests or personal relationships that could have appeared to influence the work reported in this paper.

Acknowledgments

Gadhamshetty acknowledges the funding support from the National Science Foundation, United States (BuG ReMeDEE Award # 1736255) and National Aeronautics and Space Administration, United States (NASA # NNX16AQ98A).

Appendix A. Supplementary data

Supplementary data to this article can be found online at https://doi.org/10.1016/j.biortech.2020.124398.

References

Al-Taho, N.M., Cornish, A., Warner, P.J., 1990. Molecular cloning of the methanol dehydrogenase structural gene from *Methylosinus trichosporium* OB3b. Curr. Microbiol. 20, 153–157. https://doi.org/10.1007/BF02091990.

Anthony, C., 1986. Bacterial oxidation of methane and methanol. Adv. Microb. Physiol. 27, 113–210. https://doi.org/10.1016/S0065-2911(08)60305-7.

Basotra, N., Dhiman, S.S., Agrawal, D., Sani, R.K., Tsang, A., Chadha, B.S., 2019. Characterization of a novel lytic polysaccharide monooxygenase from *Malbranchea cinnamomea* exhibiting dual catalytic behavior. Carbohydr. Res. 478, 46–53. https://doi.org/10.1016/j.carres.2019.04.006.

Bastviken, D., Cole, J.J., Pace, M.L., Van de Bogert, M.C., 2008. Fates of methane from different lake habitats: connecting whole-lake budgets and CH_4 emissions. J. Geophys. Res. 113, 1–13. https://doi.org/10.1029/2007JG000608.

Bertini, I., Cavallaro, G., Rosato, A., 2006. Cytochrome c: occurrence and functions. Chem. Rev. 106, 90–115. https://doi.org/10.1021/cr050241v.

Bordel, S., Rodríguez, Y., Hakobyan, A., Rodríguez, E., Lebrero, R., Muñoz, R., 2019a. Genome scale metabolic modeling reveals the metabolic potential of three Type II methanotrophs of the genus *Methylocystis*. Metab. Eng. 54, 191–199. https://doi.org/10.1016/j.ymben.2019.04.001.

Bordel, S., Rojas, A., Muñoz, R., 2019b. Reconstruction of a genome scale metabolic model of the polyhydroxybutyrate producing methanotroph *Methylocystis parvus* OBBP. Microb. Cell Fact. 18, 1–11. https://doi.org/10.1186/s12934-019-1154-5.

Bowman, J.P., Sayler, G.S., 1994. Optimization and maintenance of soluble methane monooxygenase activity in *Methylosinus trichosporium* OB3b. Biodegradation 5, 1–11. https://doi.org/10.1007/BF00695208.

Brooks, B.R., Bruccoleri, R.E., Olafson, B.D., States, D.J., Swaminathan, S., Karplus, M., 1983. CHARMM: a program for macromolecular energy, minimization, and dynamics calculations. J. Comput. Chem. 4, 187–217. https://doi.org/10.1002/jcc.540040211.

Chen, J.i., Sheng, K., Luo, P., Li, C., Shi, G., 2012. Graphene hydrogels deposited in nickel foams for high-rate electrochemical capacitors. Adv. Mater. 24, 4569–4573. https://doi.org/10.1002/adma.201201978.

Davamani, V., Parameswari, E., Arulmani, S., 2020. Mitigation of methane gas emissions in flooded paddy soil through the utilization of methanotrophs. Sci. Total Environ. 726, 138570. https://doi.org/10.1016/j.scitotenv.2020.138570.

Dedysh, S.N., Didriksen, A., Danilova, O.V., Belova, S.E., Liebner, S., Svenning, M.M., 2015. *Methylocapsa palsarum* sp. nov., a methanotroph isolated from a subarctic discontinuous permafrost ecosystem. Int. J. Syst. Evol. Microbiol. 65, 3618–3624. https://doi.org/10.1099/ijsem.0.000465.

Dwyer, D.S., 2005. Electronic properties of amino acid side chains: quantum mechanics calculation of substituent effects. BMC Chem. Biol. 5, 1–11. https://doi.org/10.1186/1472-6769-5-2.

Ferenci, T., 1974. Carbon monoxide-stimulated respiration in methane-utilizing bacteria. FEBS Lett. 41, 94–98. https://doi.org/10.1016/0014-5793(74)80962-2.

Gagnon, J.K., Law, S.M., Brooks 3rd, C.L., 2016. Flexible CDOCKER: Development and application of a pseudo-explicit structure-based docking method within CHARMM. J. Comput. Chem. 37, 753–762. https://doi.org/10.1002/jcc.24259.

Hanson, R.S., Hanson, T.E., 1996. Methanotrophic bacteria. Microbiol. Rev. 60, 439–471.

Harbitz, E., Andersson, K.K., 2011. Cytochrome c-554 from *Methylosinus trichosporium* OB3b; a protein that belongs to the cytochrome c2 family and exhibits a HALS-type EPR signal. PLoS One 6. https://doi.org/10.1371/journal.pone.0022014.

Haynes, C.A., Gonzalez, R., 2014. Rethinking biological activation of methane and conversion to liquid fuels. Nat. Chem. Biol. 10, 331–339. https://doi.org/10.1038/nchembio.1509.

Howarth, R.W., Santoro, R., Ingraffea, A., 2011. Methane and the greenhouse-gas footprint of natural gas from shale formations: a letter. Clim. Change 106, 679–690. https://doi.org/10.1007/s10584-011-0061-5.

Islam, J., Chilkoor, G., Jawaharraj, K., Dhiman, S.S., Sani, R., Gadhamshetty, V., 2020. Vitamin-C-enabled reduced graphene oxide chemistry for tuning biofilm phenotypes of methylotrophs on nickel electrodes in microbial fuel cells. Bioresour. Technol. 300, 122642. https://doi.org/10.1016/j.biortech.2019.122642.

Jawaharraj, K., Shrestha, N., Chilkoor, G., Dhiman, S.S., Islam, J., Gadhamshetty, V., 2020a. Valorization of methane from environmental engineering applications: A critical review. Water Res. 187, 116400 https://doi.org/10.1016/j.watres.2020.116400.

Jawaharraj, K., Shrestha, N., Chilkoor, G., Vemuri, B., Gadhamshetty, V., 2020b. Electricity from methanol using indigenous methylotrophs from hydraulic fracturing flowback water. Bioelectrochemistry 135, 107549. https://doi.org/10.1016/j.bioelechem.2020.107549.

Kumar, R., Mehta, B.R., Bhatnagar, M., S, R., Mahapatra, S., Salkalachen, S., Jhawar, P., 2014. Graphene as a transparent conducting and surface field layer in planar Si solar cells. Nanoscale Res. Lett. 9, 349. https://doi.org/10.1186/1556-276X-9-349.

Lucas, M.F., Rousseau, D.L., Guallar, V., 2011. Electron transfer pathways in cytochrome c oxidase. Biochim. Biophys. Acta 1807, 1305–1313. https://doi.org/10.1016/j.bbabio.2011.03.003.Electron.

McAnulty, M.J., Poosarla, V.G., Kim, K.-Y., Jasso-Chávez, R., Logan, B.E., Wood, T.K., 2017. Electricity from methane by reversing methanogenesis. Nat. Commun. 8 https://doi.org/10.1038/ncomms15419.

Mcdonald, I.R., Murrell, J.C., 1997. The methanol dehydrogenase structural gene mxaf and its use as a functional gene probe for methanotrophs and methylotrophs. Appl. Environ. Microbiol. 63, 3218–3224. https://doi.org/10.1128/aem.63.8.3218-3224.1997.

Naizabekov, S., Lee, E.Y., 2020. Genome-scale metabolic model reconstruction and in silico investigations of methane metabolism in *Methylosinus trichosporium* Ob3b. Microorganisms 8, 437. https://doi.org/10.3390/microorganisms8030437.

Priyadarsini, S., Mohanty, S., Mukherjee, S., Basu, S., Mishra, M., 2018. Graphene and graphene oxide as nanomaterials for medicine and biology application. J. Nanostruct. Chem. 8, 123–137. https://doi.org/10.1007/s40097-018-0265-6.

Roslev, P., King, G.M., 1995. Aerobic and anaerobic starvation metabolism in methanotrophic bacteria. Appl. Environ. Microbiol. 61, 1563–1570. https://doi.org/10.1128/aem.61.4.1563-1570.1995.

Semrau, J.D., DiSpirito, A.A., Gu, W., Yoon, S., 2018. Metals. https://doi.org/10.1128/AEM.02289-17.

Shrestha, N., Chilkoor, G., Wilder, J., Gadhamshetty, V., Stone, J.J., 2017. Potential water resource impacts of hydraulic fracturing from unconventional oil production in the Bakken shale. Water Res. 108, 1–24. https://doi.org/10.1016/j.watres.2016.11.006.

Slate, A.J., Whitehead, K.A., Brownson, D.A.C., Banks, C.E., 2019. Microbial fuel cells: an overview of current technology. Renew. Sustain. Energy Rev. 101, 60–81. https://doi.org/10.1016/j.rser.2018.09.044.

Tanaka, K., Yokoe, S., Igarashi, K., Takashino, M., Ishikawa, M., Hori, K., Nakanishi, S., Kato, S., 2018. Extracellular electron transfer via outer membrane cytochromes in a methanotrophic bacterium *Methylococcus capsulatus* (Bath). Front. Microbiol. 9, 1–7. https://doi.org/10.3389/fmicb.2018.02905.

Tokunou, Y., Hashimoto, K., Okamoto, A., 2016. Acceleration of extracellular electron transfer by alternative redox-active molecules to riboflavin for outer-membrane cytochrome c of *Shewanella oneidensis* MR-1. J. Phys. Chem. C 120, 16168–16173. https://doi.org/10.1021/acs.jpcc.6b00349.s001.

Tonge, G.M., Knowles, C.J., Harrison, D.E.F., Higgins, I.J., 1974. Metabolism of one carbon compounds: cytochromes of methane and methanol-utilising bacteria. FEBS Lett. 44, 106–110. https://doi.org/10.1016/0014-5793(74)80316-9.

Wang, H., Wang, G., Ling, Y., Qian, F., Song, Y., Lu, X., Chen, S., Tong, Y., Li, Y., 2013. High power density microbial fuel cell with flexible 3D graphene–nickel foam as anode. Nanoscale 5, 10283. https://doi.org/10.1039/c3nr03487a.

Watowich, S.J., Meyer, E.S., Hagstrom, R., Josephs, R., 1988. A stable, rapidly converging conjugate gradient method for energy minimization. J. Comput. Chem. 9, 650–661. https://doi.org/10.1002/jcc.540090611.

Xin, Z., Zeyang, Y., Daling, G., Gonglei, W., Wei, Z., 2020. Metagenome metabolic analysis revealing the mechanism of simultaneous methanogenesis, aerobic methane oxidation and denitrification (SMAMOD) in a microaerobic up-flow sludge bed biofilm reactor. J. Chem. Technol. Biotechnol. 95, 2229–2236. https://doi.org/10.1002/jctb.6410.

Yang, Y., Tong, T., Chen, J., Liu, Y., Xie, S., 2020. Ammonium impacts methane oxidation and methanotrophic community in freshwater sediment. Front. Bioeng. Biotechnol. 8, 1–11. https://doi.org/10.3389/fbioe.2020.00250.

Zhang, Y.-W., Tiwari, M.K., Gao, H., Dhiman, S.S., Jeya, M., Lee, J.-K., 2012. Cloning and characterization of a thermostable H_2O-forming NADH oxidase from *Lactobacillus rhamnosus*. Enzyme Microb. Technol. 50, 255–262. https://doi.org/10.1016/j.enzmictec.2012.01.009.

Zhou, S., Tang, J., Yuan, Y., Yang, G., Xing, B., 2018. TiO_2 nanoparticle-induced nanowire formation facilitates extracellular electron transfer. Environ. Sci. Technol. Lett. 5, 564–570. https://doi.org/10.1021/acs.estlett.8b00275.s001.